

# Fundamental Limit of the Emission Linewidths of Quantum Dots: An Ab Initio Study of CdSe Nanocrystals

Sungwoo Kang, Yongwook Kim, Eunjoo Jang,\* Youngho Kang,\* and Seungwu Han\*

Cite This: *ACS Appl. Mater. Interfaces* 2020, 12, 22012–22018

Read Online

ACCESS |



Metrics &amp; More



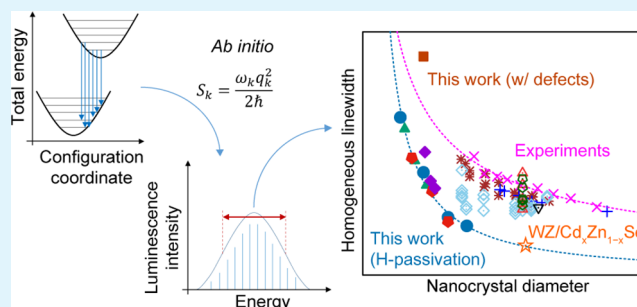
Article Recommendations



Supporting Information

**ABSTRACT:** The emission linewidth of a semiconducting nanocrystal (NC) significantly affects its performance in light-emitting applications, but its fundamental limit is still elusive. Herein, we analyze the exciton–phonon coupling (EPC) from Huang–Rhys (HR) factors using ab initio calculations and compute emission line shapes of CdSe NCs. When surface traps are absent, acoustic modes are found to dominate EPC. The computed linewidths are mainly determined by the size of NCs, being largely insensitive to the shape and crystal structure. Linewidths obtained in this work are much smaller than most measurements on homogeneous linewidths, but they are consistent with a CdSe/Cd<sub>x</sub>Zn<sub>1-x</sub>Se (core/shell) NC [Park, Y.-S.; Lim, J.; Klimov, V. I. *Nat. Mater.* 2019 18, 249–255]. Based on this comparison, it is concluded that the large linewidths in most experiments originated from internal fields by surface (or interface) traps or quasi-type II band alignment that amplifies EPC. Thus, the present results on NCs with ideal passivation provide the fundamental minimum of homogeneous linewidths, indicating that only the CdSe/Cd<sub>x</sub>Zn<sub>1-x</sub>Se NC has achieved this limit through well-controlled synthesis of shell structures. To further verify the role of internal fields, we model NCs with charged surface defects. We find that the internal field significantly increases HR factors and linewidths, in reasonable agreement with experiments on single cores. By revealing the fundamental limit of the emission linewidths of quantum dots, this work will pave the way for engineering quantum dots with an ultrasharp spectrum.

**KEYWORDS:** quantum dots, nanocrystals, density functional theory, exciton–phonon coupling, homogeneous linewidth, photoluminescence, electroluminescence, surface traps



## 1. INTRODUCTION

Due to the high luminescence efficiency and size-dependent tunability of emission wavelength, semiconductor nanocrystals (NCs) hold great potential as light emitters for display,<sup>1</sup> biological labeling,<sup>2</sup> and laser applications.<sup>3</sup> For optimal performance in these applications, sharp emission spectra of NCs are essential. In particular, for the display application, the color purity of red, green, and blue (RGB)—three primary colors—affects the color gamut of displays.<sup>4</sup> Therefore, significant research efforts are directed toward narrowing the luminescence linewidth of NC ensembles.

The spectral linewidth of an NC ensemble is controlled by two sources, namely, homogeneous and inhomogeneous. The inhomogeneous source is associated with nonuniformity in the NC size, which leads to a broad distribution of the emission wavelength from individual NCs.<sup>5</sup> On the other hand, homogeneous sources relate to the finite width of the optical spectrum from single NCs. Homogeneous broadening is known to originate from exciton–phonon coupling (EPC), exciton fine structures, and spectral dynamics. Among these sources, EPC is known to play the most significant role.<sup>6–9</sup>

Over the last few decades, synthetic methods have been advanced to produce a highly uniform batch of NCs.<sup>4,10,11</sup> Recently, by controlling the epitaxial shell growth with entropic ligands, Zhou et al. synthesized ensembles of CdSe/CdS (core/shell) NCs possessing the photoluminescence (PL) linewidth equivalent to that of single quantum dots.<sup>12</sup> This means that inhomogeneous broadening can be suppressed sufficiently by advanced synthetic methods. On the other hand, the linewidth of single NCs and the influence of EPC have been extensively studied for CdSe NCs using several spectroscopy techniques such as single-particle photoluminescence spectroscopy,<sup>13,14</sup> photon-correlation Fourier spectroscopy,<sup>15</sup> and multidimensional electronic spectroscopy.<sup>9</sup> However, the measured full-width at half maximum (FWHM) of the emission spectra showed a wide range even for CdSe NCs

Received: February 14, 2020

Accepted: April 16, 2020

Published: April 16, 2020



with similar dimensions; previous studies showed a FWHM of 50–100 meV at room temperature<sup>8,9,16</sup> while a more recent work by Park et al. reported a far narrower linewidth of 24 meV.<sup>17</sup> In addition, the relative importance between acoustic and optical phonons is still under debate; Liptay et al. emphasized the exciton-acoustic phonon coupling in explaining the spectral linewidth of NCs,<sup>18</sup> while Cui et al. and Gellen et al. pointed out the Fröhlich coupling with optical modes as the origin of spectral broadening.<sup>8,9</sup> Thus, the fundamental understanding of the intrinsic linewidth is still incomplete, and its ultimate limit remains elusive.

Theoretical estimation of the emission spectra of NCs can shed light on the origin of homogeneous broadening and help in identifying the fundamental limit of the spectral linewidth of NCs. For instance, spectral broadening of NCs by exciton-phonon coupling was calculated by assuming that NCs elastically vibrate like continuous particles.<sup>19,20</sup> However, such continuum methods cannot capture atomistic effects on exciton-phonon coupling such as surface defects and hydrostatic strain in core/shell quantum dots. Patrick et al. calculated the absorption spectra of diamondoids using first-principles calculations by evaluating Condon integrals by Monte Carlo techniques, and the obtained results agree well with experiments.<sup>21</sup> However, this approach may not be compatible with NCs (hundreds to thousands of atoms) that have a large degree of freedom in atomic configurations.

In this work, motivated by the absence of a fully ab initio study on the FWHM of actual-scale quantum dots, we develop a computational method based on the Franck-Condon approximation and the density functional theory (DFT) and apply the method to evaluate luminescence line shapes of NCs. To the best of our knowledge, this is the first attempt to evaluate the emission linewidths of NCs using ab initio methods. For specific material systems, we focus on CdSe NCs because of rich experimental data, but the computational method developed here can be applied to NCs in general. We first study ideal CdSe NCs, whose surface is fully passivated by pseudo-hydrogen atoms. The EPC is defined in terms of Huang-Rhys (HR) factors, and it is found that acoustic modes contribute the most to the spectral broadening of the NC models. We also demonstrate that the spectral linewidth strongly depends on the size of NCs and to a lesser extent on the morphologies and crystal structures. We find that the calculated FWHM is consistent with the result of the latest single-particle measurement for CdSe/Cd<sub>x</sub>Zn<sub>1-x</sub>Se core/shell NC. Charged defects on the NC surface are also modeled, and it is shown that the surface defects produce an internal electric field, significantly enhancing EPC and the FWHM.

## 2. METHOD

**2.1. Calculation of Luminescence Spectra.** We first develop a microscopic theory of luminescence. When the dipole moment of the electronic transition is independent of atomic coordinates (the Franck-Condon approximation), the normalized luminescence intensity or the line shape for a single level of the exciton state is given by<sup>22</sup>

$$I(\omega) = C\omega^3 A(\omega) \quad (1)$$

where  $C$  is the normalization constant and  $\omega$  is the frequency of emitted photons. In eq 1,  $A(\omega)$  is a spectral function related to phonon transitions during the optical emission. A direct calculation of  $A(\omega)$  is computationally demanding for NCs

with more than hundreds of atoms because it involves complicated multidimensional integrals. We simplify the computation by employing a parallel approximation in which phonon eigenmodes are assumed to be identical in the ground and excited states despite shifts in atomic coordinates (see Figure 1a) (we confirm that the phonon spectrum is similar

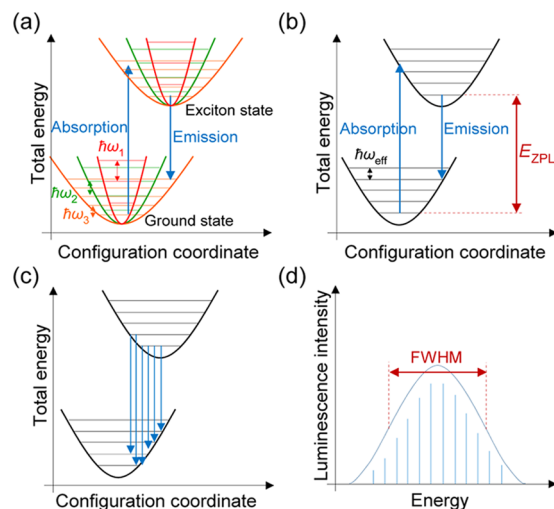


**Figure 1.** Schematic representation of exciton-phonon coupling. Configuration coordinate of (a) all modes and (b) single mode reduced by the effective-mode approximation. (c) The configuration coordinate diagram describing optical broadening of the emission spectrum. (d) Schematic representation of line spectrum broadened by exciton-phonon coupling.

between the ground and excited states, as shown in Figures S1 and S2).<sup>23</sup> Note that this approximation will not be valid if structural distortions during the vertical transition are significant such that phonon modes are distinct between the ground and excited states (for instance, the peroxide formation in ZnO).<sup>24</sup> Within the parallel approximation,  $A(\omega)$  is written as

$$A(\omega) = \sum_{\{l_k\}} \left[ \prod_k \sum_m w_{km}(T) |\chi_{k(m+l_k)}^g \chi_{km}^e|^2 \right] \times \delta \left( E_{ZPL} - \sum_k l_k \hbar \omega_k - \hbar \omega \right) \quad (2)$$

where  $E_{ZPL}$  is the energy of zero-phonon line (see Figure 1b),  $k$  is the index for phonon modes,  $\chi_{k(m+l_k)}^g$  and  $\chi_{km}^e$  are vibrational wave functions of the ground and excited states, respectively, and  $m$  and  $(m + l_k)$  indicate the phonon index for each mode. In eq 2,  $\{l_k\}$  is a set of different combinations of  $l_k$  and  $w_{km}(T)$  is the thermal occupation of  $\chi_{km}^e$  state at a given temperature  $T$ . In eq 2, broadening of the zero-phonon line, which is related to phonon damping effects,<sup>25–27</sup> is neglected. Owing to the parallel approximation, the thermal average of the overlap integral over excited states in eq 2 can be expressed analytically in terms of HR factors<sup>28</sup>

$$\begin{aligned} & \sum_m w_{km}(T) |\langle \chi_{km}^g | \chi_{k(m+l_k)}^e \rangle|^2 \\ &= \exp \left\{ \frac{I_k \hbar \omega_k}{2k_b T} - S_k \coth \left( \frac{\hbar \omega_k}{2k_b T} \right) \right\} \\ & \quad \times I_{I_k} \left\{ S_k / \sinh \left( \frac{\hbar \omega_k}{2k_b T} \right) \right\} \end{aligned} \quad (3)$$

where  $k_b$  is the Boltzmann constant and  $I_k$  is the modified Bessel function. In eq 3,  $S_k$  is the partial Huang–Rhys factor of the  $k$ th phonon mode, which is defined as<sup>29</sup>

$$S_k = \frac{\omega_k q_k^2}{2\hbar} \quad (4)$$

where  $q_k$  is the projection of the structural change induced by the electronic transition onto the phonon eigenmodes, given by

$$q_k = \sum_{\alpha} m_{\alpha}^{1/2} [\vec{R}_{\alpha}(\alpha) - \vec{R}_{\alpha}(\alpha)] \times \vec{n}_k(\alpha) \quad (5)$$

In eq 5,  $m_{\alpha}$  is the mass of atom  $\alpha$ ,  $\vec{R}_{\alpha}(\alpha)$  ( $\vec{R}_{\alpha}(\alpha)$ ) is the atomic coordinate of atom  $\alpha$  in the ground (excited) state, and  $\vec{n}_k(\alpha)$  is the normalized phonon eigenvector. Equations 4 and 5 were used in a previous study to evaluate partial HR factors for Si, C, InAs, and CdSe NCs.<sup>30</sup>

The parallel approximation significantly simplifies the computation of overlap integrals in eq 2. Nevertheless, the computational cost to evaluate eq 2 grows rapidly with NC size due to the increasing number of phonon modes. Therefore, further approximation is necessary to obtain the luminescence spectrum for large NCs. Herein, we introduce an effective vibrational mode (see Figure 1b). The frequency of this effective mode is obtained by taking the average value of the frequency squares of phonon modes as follows<sup>23</sup>

$$\omega_{\text{eff}}^2 = \sum_k p_k \omega_k^2 \quad (6)$$

where  $p_k$  is a partial weight representing the contribution of mode  $k$  to the lattice distortion during the optical transition, i.e.,  $p_k = q_k^2 / \sum_k q_k^2$ . Then, the effective Huang–Rhys factor ( $S_{\text{eff}}$ ) is given by

$$S_{\text{eff}} = \frac{\sum_k S_k \hbar \omega_k}{\hbar \omega_{\text{eff}}} \quad (7)$$

The effective-mode approach was successfully applied to study the luminescence spectra of defects in ZnO and GaN.<sup>23</sup> In contrast to the previous work that focused on vibrations of the atoms in the vicinity of defects,<sup>23</sup> we take into account vibrations of every atom in NCs when calculating the properties related to the effective mode. Moreover, we consider excitonic effects although at the single-particle level (see Section 2.2). In Figure S3, we confirm that this method yields emission line shapes comparable to those obtained by considering the full spectrum of vibrational modes.

We replace  $\delta$ -function in eq 2 with a Gaussian smeared with widths of 2–7 meV (see the Supporting Information for details), which is smaller than 10% of the FWHM of the line spectra resulting from EPC. The possible optical transitions and the resulting luminescence spectrum are schematically illustrated in Figure 1c,d, respectively.

**2.2. Computational Setup.** The optimized atomic geometries, electronic structures, and vibrational spectra of CdSe NCs are obtained by DFT calculations using Vienna ab initio simulation package (VASP)<sup>31</sup> with the projector augmented wave (PAW) method.<sup>32</sup> We employ the generalized gradient approximation for the exchange–correlation functional with Hubbard  $U$  corrections ( $U = 9.5$  eV for Cd 4d states).<sup>33,34</sup> This computational scheme produces a linewidth similar to that of more accurate but expensive hybrid functional calculations (see Figures S4 and S5). The excited state is simulated by constrained DFT, in which the electron occupation of the highest occupied molecular orbital (HOMO) and the lowest unoccupied molecular orbital (LUMO) is regulated to mimic an excitonic state.<sup>35–37</sup> This approach was reported to yield a reorganization energy during the optical transition in Si NCs comparable to that of advanced approaches such as quantum Monte Carlo (QMC) and time-dependent DFT.<sup>36</sup> We assume that the excited state forms a spin triplet state ( $|\uparrow\uparrow\rangle$ ), but the results barely change with a specific spin configuration (singlet or triplet). The spin–orbit coupling (SOC) is not included because it is negligible (see Figure S6). In emulating the excitonic state, three highest occupied levels are evenly emptied because their energies are almost degenerate.<sup>36,38</sup> Details of computational parameters and procedures are provided in the Supporting Information.

### 3. RESULTS AND DISCUSSION

To reveal which phonon modes are critical for the luminescence linewidth, we analyze  $S_k$  of four different types of CdSe NCs with similar diameters ( $D_s$ ) of 1.3–1.7 nm as shown in Figure 2a–d: (a) spherical zinc-blende (sp-ZB), (b)

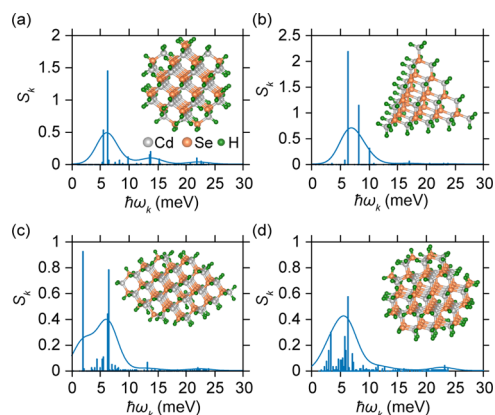


**Figure 2.** Partial Huang–Rhys factors ( $S_k$ ) of (a) sp-ZB ( $D = 1.5$  nm), (b) td-ZB ( $D = 1.3$  nm), (c) spo-ZB ( $D = 1.7$  nm), and (d) sp-WZ ( $D = 1.7$  nm) CdSe NCs. The vertical lines represent the partial Huang–Rhys factor for each mode, which are smeared ( $\sigma = 1.7$  meV) into a continuous envelope. Atomic structures are presented as the inset. Gray atoms are Cd, orange atoms are Se, and green atoms are pseudo-hydrogen.

tetrahedral zinc-blende (td-ZB), (c) spheroidal zinc-blende (spo-ZB), and (d) spherical wurtzite (sp-WZ) NCs. Here,  $D$  is defined as twice the average distance from the center of NCs to the Cd and Se atoms on the NC surface. Dangling bonds of surface Cd (Se) ions are passivated by pseudo-hydrogen with a charge of  $1.5e^-$  ( $0.5e^-$ ). The fractional charges are chosen to satisfy the charge neutrality. In Figure 2, we find that the HR factors of every NC are mostly contributed by phonons with energies less than 15 meV, indicating that the exciton mainly

couples with acoustic modes. The strong EPC of acoustic modes is associated with the nature of electronic wave functions of the HOMO and the LUMO; the HOMO in CdSe is mainly formed by the nonbonding state of Se 4p orbitals (see Figure 3a), while the LUMO consists of an

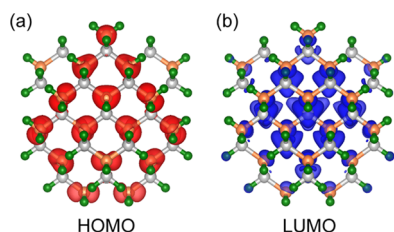


**Figure 3.** Partial charges of (a) HOMO and (b) LUMO states of sp-ZB CdSe NCs with a diameter of 1.49 nm.

antibonding state between Cd 5s and Se 4s orbitals (see Figure 3b). Upon exciton formation, the lattice expands slightly because of the antibonding nature of the LUMO, and this lattice expansion involves the atomic motion akin to acoustic modes, particularly longitudinal ones (see Movie S1).

For the spo-ZB NC, it is seen that an ellipsoidal acoustic mode at  $\sim 2$  meV (see Movie S2) produces large EPC due to the asymmetric shape. This finding is consistent with a recent experiment in which relative contributions of vibrational modes to spectral broadening were resolved using three-dimensional electronic spectroscopy for CdSe NCs with aspect ratios of 1.1–1.3.<sup>9</sup>

Figure 4a shows the  $S_{\text{eff}}$  of NCs as a function of  $D$ . Because of similar distributions of the partial HR factors regardless of NC shapes (see Figure 2),  $S_{\text{eff}}$  in the present study mainly depends on the size of the NCs, and it decreases with  $D$ . In the case of sp-ZB NCs, the dependence is fitted to  $D^{-1.8}$ . This is consistent with  $D^{-2}$  from a continuum model for spherical CdSe NCs, which considered deformation potentials for EPC.<sup>19</sup> The inverse correlation between  $S_{\text{eff}}$  and  $D$  can be understood by the fact that HOMO and LUMO states are spread over more atoms in larger NCs, which results in a smaller lattice distortion upon exciton formation.

Based on  $S_{\text{eff}}$  we calculate the spectral line shape of the CdSe NCs using eq 2, as shown in Figure 4b for sp-ZB NCs with various sizes at room temperature (300 K).  $E_{\text{ZPE}}$  in eq 2 is adjusted to match with the peak position in experiments.<sup>39</sup> In Figure 4c, we plot the FWHMs obtained from the calculated spectra. As expected by smaller  $S_{\text{eff}}$  for NCs with larger sizes, the luminescence spectra become narrower with increasing NC size. From fitting of the data for sp-ZB NCs, it is found that FWHM scales with  $\sim D^{-1.3}$  (blue dotted line). In comparison with sp-ZB NCs, the FWHMs for sp-WZ NCs decay more quickly with increasing  $D$ . This is because the EPC in sp-WZ NCs is stronger than that in sp-ZB NCs when  $D$  is small, which in turn originates from a lower symmetry in the wurtzite structure that results in lesser sphericity in the NC shape (see Figure S7). However, the sphericity of sp-WZ NCs increases with  $D$ , and the spectral linewidth of sp-WZ approaches that of sp-ZB NCs (see Figure S8). On the other hand, the data for sp-WZ NCs cannot be described by a simple power law because the sphericity changes gradually with  $D$ .

In Figure 4c, we compare the calculated FWHMs with homogeneous linewidths measured for CdSe NCs with core/shell structures. Most of experiments except for Park et al.<sup>17</sup> reported FWHMs ( $>50$  meV) that are greater than the present

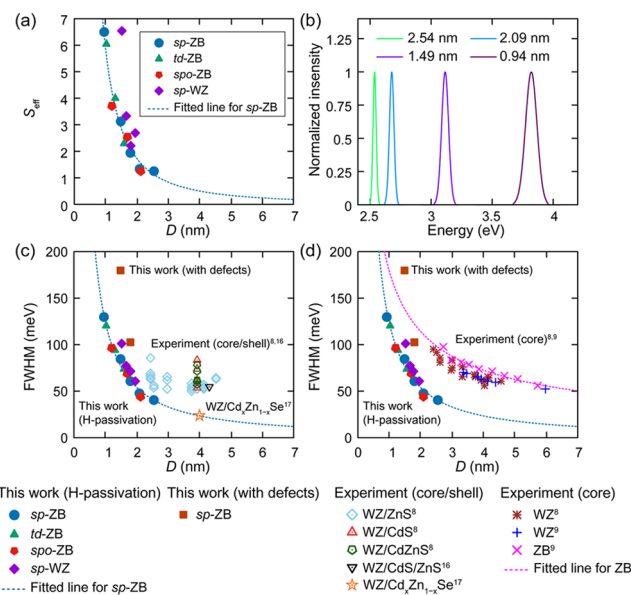


**Figure 4.** (a) Effective Huang–Rhys factor of CdSe NCs as a function of core diameter ( $D$ ). (b) Line shape of various sizes of sp-ZB NCs at 300 K, and the legend represents  $D$  of each NCs. The linewidth, calculated at 300 K, as a function of  $D$  compared with experimental measurement of the homogeneous linewidths of (c) core<sup>8,9</sup> and (d) core/shell CdSe NCs.<sup>8,16,17</sup> Linewidth data computed in this work presented in (d) is repeated from (c). Legends of (c) and (d) are shown integrated below the figure. The core diameters of experimental NCs are deduced from the first absorption peak using an empirical fitting function<sup>39</sup> if they are not stated in the literature. The dotted lines in (a), (c), and (d) are fitted to  $aD^{-x}$ , where  $a$  and  $x$  are fitting constants. Reproduced with permission from ref 8. Copyright 2016 American Chemical Society. Reproduced with permission from ref 9. Copyright 2017 American Chemical Society. Reproduced with permission from ref 16. Copyright 2006 AIP Publishing. Reproduced with permission from ref 17. Copyright 2019 Springer Nature. Reproduced with permission from ref 39. Copyright 2003 American Chemical Society.

theoretical estimation. We attribute the larger values in experiments to the two additional factors that are not considered in the present calculations: (1) internal field due to the lattice-mismatch-induced traps (CdSe/ZnS) and (2) quasi-type II band alignment between core and shell materials (CdSe/CdS, CdSe/CdZnS, CdSe/CdS/ZnS) in which the electron wave function of CdSe extends into the shell region.<sup>8</sup> In contrast, Park et al. optimized the composition of  $\text{Cd}_x\text{Zn}_{1-x}\text{Se}$  shells to avoid the lattice mismatch while maintaining type-I band alignment such that both the HOMO and LUMO of CdSe are well confined in the core region.<sup>17</sup> Therefore, the optical emission of this NC is mainly determined by the core material, which is consistent with the present computational model. Indeed, they obtained an FWHM of 24 meV, which coincides with the theoretical estimation of 23 meV extrapolated by the fitted scaling relation for sp-ZB NCs. To note, calculated FWHMs of sp-ZB and sp-WZ NCs become similar at large  $D$ , with only a 10% difference at  $D = 2.0$  nm. Therefore, the comparison of theoretical values for sp-ZB NCs with those for WZ CdSe in Park et al. would be valid.

On the other hand, experimental PL linewidths for CdSe NCs whose surfaces are stabilized by organic ligands overestimate the calculated values (see Figure 4d). The larger broadening in experiments would be attributed to the

incomplete passivation of surface traps, which causes an internal electric field inside of NCs.<sup>9</sup> To investigate the effect of surface traps, we examine the line shape of defective sp-ZB NCs with  $D = 1.5$  and  $1.8$  nm, wherein a pair of hydrogen atoms is eliminated, thereby leaving dangling bonds of the Cd and Se atoms at the opposite sides of the surface (see Figure 5a

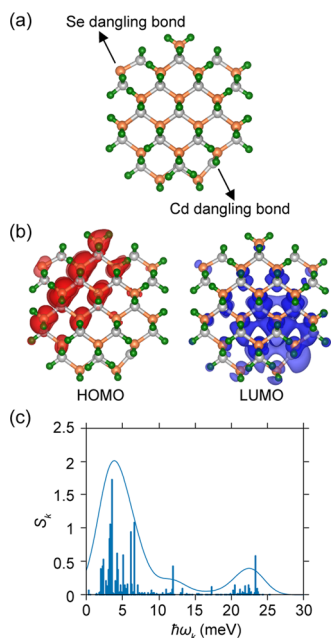


**Figure 5.** (a) Atomic structure, (b) partial charge of the HOMO and the LUMO, and (c) partial Huang–Rhys factors of the 1.49 nm sp-ZB NC with surface defects.

for the defective NC with  $D = 1.5$  nm). When the Cd and Se dangling bonds are closer to each other, the linewidth becomes narrower due to weakened internal fields (see Figure S9 and Table S1). Therefore, the defect arrangement we adopt here may correspond to an extreme case that provides an upper limit of the linewidth in the presence of two dangling bonds on the surface. The localized defect level associated with the Cd dangling bond lies above the LUMO, while the one for the Se dangling bond appears within the HOMO–LUMO gap. Therefore, one electron in the Cd state transfers to Se sites, which results in the empty Cd state ( $\text{Cd}^{2+}$ ) and fully occupied Se state ( $\text{Se}^{2-}$ ). Here, we assume that the charge states of defects are maintained during emission.<sup>9,18,40,41</sup>

The computed FWHMs of the defective models are marked as red solid squares in Figure 4c,d. It is intriguing that the linewidth of the NCs with  $D$  values of 1.5 and 1.8 nm increase from 84 to 180 meV and from 55 to 103 meV, respectively, when the surface defects are present. The increased FWHMs are in a reasonable agreement with the dashed line in Figure 4d that is obtained by fitting the experimental FWHMs for CdSe single cores (zinc-blende structures).<sup>9</sup> The microscopic origin underlying the large linewidth in the defective NC is the spatial separation of the HOMO and LUMO states due to polarization. As shown in Figure 5b, the HOMO (LUMO) state is weighted toward the atomic site of Se (Cd) with a dangling bond. Consequently, the structural distortion upon electronic excitation becomes more severe than that for ideally passivated NCs, resulting in larger HR factors (see Figure 5c). In particular, optical modes also play a role in this case.

We notice that the experimental data in refs 8 and 9 are found to scale with  $D^{-0.7}$  and  $D^{-0.6}$ , respectively, which are rather weaker dependence compared to our result for defect-free NCs ( $\sim D^{-1.3}$ ). These discrepancies might be attributed to the fact that surface defects play a crucial role in determining the linewidths in experiments. The size dependence of defective NCs would be a subject in future studies.

So far, we have compared our results with the data from PL experiments. It can be questioned whether the present results can also be compared with electroluminescence (EL) measurements, noting that carrier densities could be different between the two measurement methods. Specifically, in EL measurements, electrons or holes can accumulate in active layers due to unbalanced carrier injections and affect luminescence characteristics of NCs. However, recent EL and PL measurements reported the same spectral linewidth for InP/ZnSe/ZnS NCs.<sup>42</sup> Nevertheless, the dominance of a single carrier type in EL can suppress radiative recombination by increasing the probability of Auger recombination.<sup>43</sup>

Finally, we investigate the temperature dependence of the emission linewidth at high temperatures ( $>40$  K), where phonon sidebands play an important role in determining the luminescence line shape of NCs. (At very low temperatures, the zero-phonon emission is also crucial for the line shape.)<sup>25</sup> To this end, we examine the line shapes of sp-ZB NCs ( $D = 1.8$  nm) with and without a pair of Cd and Se dangling bonds on the surface at different temperatures ( $T$ ), and the results are compared to the experimental measurement on the ensemble linewidths of similar-sized CdSe NCs ( $D = 2.2$  nm)<sup>44</sup> (see Figure 6). The defective NC has greater  $T$ -dependence than

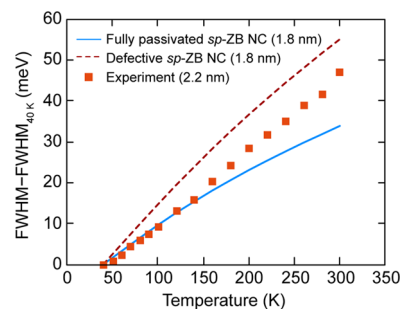


**Figure 6.** Temperature dependence of the linewidth of a fully passivated and defective sp-ZB NC ( $D = 1.8$  nm) with a pair of Cd and Se dangling bonds on the surface compared to the measurement on the ensemble linewidth of the commercial CdSe NC ( $D = 2.2$  nm).<sup>44</sup> Each FWHM is offset by its value at 40 K. Reproduced with permission from ref 44. Copyright 2017 American Chemical Society.

the fully passivated NC, which can be understood by stronger exciton–phonon coupling when NCs have defects. We also find that the experimental  $T$ -dependence agrees better with the defective NC rather than the fully passivated one.

#### 4. CONCLUSIONS

In conclusion, we developed a computational method for evaluating the luminescence line shapes of semiconductor NCs due to EPC. By applying the method to archetypal CdSe NCs, we have demonstrated the capability of our approach to estimate spectral linewidths accurately. Based on the computational results, we provided crucial insights into the key factors for intrinsic linewidths that are not easily resolved by experiments alone, such as the coupling strength between

excitons and phonons and the effect of NC size and charged defects on the surface. This method can also be used to estimate the ultimate linewidth of nanocrystals with specific size and composition, which will be a useful reference value in experiment. The theoretical framework proposed in the present study is universal, applicable to any type of NCs. On the other hand, several aspects of emission spectrum of NCs like the detailed role of various types of defects, impacts of ligand interaction, and shell composition in core/shell NCs remain to be unclarified yet. Such topics will be the subjects of future studies. By revealing the fundamental limit of emission linewidths of quantum dots, this work will pave the way for engineering quantum dots with an ultrasharp spectrum.

## ■ ASSOCIATED CONTENT

### Supporting Information

The Supporting Information is available free of charge at <https://pubs.acs.org/doi/10.1021/acsami.0c02904>.

Details of DFT calculations, validation of the parallel approximation, effective-mode approximation, and exchange–correlation functional (PDF)

Movie of longitudinal acoustic mode of CdSe NCs (MP4)

Movie of the ellipsoidal acoustic mode of CdSe NCs (MP4)

## ■ AUTHOR INFORMATION

### Corresponding Authors

**Eunjoon Jang** – Inorganic Material Lab, Samsung Advanced Institute of Technology, Samsung Electronics, Gyeonggi-do 16678, Korea; [orcid.org/0000-0003-2573-0176](https://orcid.org/0000-0003-2573-0176); Email: [ejjang12@samsung.com](mailto:ejjang12@samsung.com)

**Youngho Kang** – Department of Materials Science and Engineering, Incheon National University, Incheon 22012, Korea; [orcid.org/0000-0003-4532-0027](https://orcid.org/0000-0003-4532-0027); Email: [youngho84@inu.ac.kr](mailto:youngho84@inu.ac.kr)

**Seungwu Han** – Department of Materials Science and Engineering, Seoul National University, Seoul 08826, Korea; [orcid.org/0000-0003-3958-0922](https://orcid.org/0000-0003-3958-0922); Email: [hansw@snu.ac.kr](mailto:hansw@snu.ac.kr)

### Authors

**Sungwoo Kang** – Department of Materials Science and Engineering, Seoul National University, Seoul 08826, Korea; [orcid.org/0000-0001-8177-8815](https://orcid.org/0000-0001-8177-8815)

**Yongwook Kim** – Inorganic Material Lab, Samsung Advanced Institute of Technology, Samsung Electronics, Gyeonggi-do 16678, Korea; [orcid.org/0000-0002-9270-5993](https://orcid.org/0000-0002-9270-5993)

Complete contact information is available at: <https://pubs.acs.org/doi/10.1021/acsami.0c02904>

### Notes

The authors declare no competing financial interest.

## ■ ACKNOWLEDGMENTS

This work was supported by the Samsung Advanced Institute of Technology (SAIT) under project no. IO181129–05781–01. The computation was carried out at the KISTI super-computing center (grant no. KSC-2018-CHA-0038).

## ■ REFERENCES

(1) Steckel, J. S.; Snee, P.; Coe-Sullivan, S.; Zimmer, J. P.; Halpert, J. E.; Anikeeva, P.; Kim, L. A.; Bulovic, V.; Bawendi, M. G. Color-

Saturated Green-Emitting QD-LEDs. *Angew. Chem., Int. Ed.* **2006**, *45*, 5796–5799.

(2) Yue, Z.; Lisdat, F.; Parak, W. J.; Hickey, S. G.; Tu, L.; Sabir, N.; Dorfs, D.; Bigall, N. C. Quantum-Dot-Based Photoelectrochemical Sensors for Chemical and Biological Detection. *ACS Appl. Mater. Interfaces* **2013**, *5*, 2800–2814.

(3) Eisler, H. J.; Sundar, V. C.; Bawendi, M. G.; Walsh, M.; Smith, H. I.; Klimov, V. Color-Selective Semiconductor Nanocrystal Laser. *Appl. Phys. Lett.* **2002**, *80*, 4614–4616.

(4) Jang, E.; Jun, S.; Jang, H.; Lim, J.; Kim, B.; Kim, Y. White-Light-Emitting Diodes with Quantum Dot Color Converters for Display Backlights. *Adv. Mater.* **2010**, *22*, 3076–3080.

(5) Peng, X.; Wickham, J.; Alivisatos, A. P. Kinetics of II-VI and III-V Colloidal Semiconductor Nanocrystal Growth: “Focusing” of Size Distributions. *J. Am. Chem. Soc.* **1998**, *120*, 5343–5344.

(6) Kelley, A. M. Electron-Phonon Coupling in CdSe Nanocrystals. *J. Phys. Chem. Lett.* **2010**, *1*, 1296–1300.

(7) Salvador, M. R.; Graham, M. W.; Scholes, G. D. Exciton-Phonon Coupling and Disorder in the Excited States of CdSe Colloidal Quantum Dots. *J. Chem. Phys.* **2006**, *125*, No. 184709.

(8) Cui, J.; Beyler, A. P.; Coropceanu, I.; Cleary, L.; Avila, T. R.; Chen, Y.; Cordero, J. M.; Heathcote, S. L.; Harris, D. K.; Chen, O.; Cao, J.; Bawendi, M. G. Evolution of the Single-Nanocrystal Photoluminescence Linewidth with Size and Shell: Implications for Exciton-Phonon Coupling and the Optimization of Spectral Linewidths. *Nano Lett.* **2016**, *16*, 289–296.

(9) Gellen, T. A.; Lem, J.; Turner, D. B. Probing Homogeneous Line Broadening in CdSe Nanocrystals Using Multidimensional Electronic Spectroscopy. *Nano Lett.* **2017**, *17*, 2809–2815.

(10) Chen, O.; Zhao, J.; Chauhan, V. P.; Cui, J.; Wong, C.; Harris, D. K.; Wei, H.; Han, H. S.; Fukumura, D.; Jain, R. K.; Bawendi, M. G. Compact High-Quality CdSe-CdS Core-Shell Nanocrystals with Narrow Emission Linewidths and Suppressed Blinking. *Nat. Mater.* **2013**, *12*, 445–451.

(11) Reiss, P.; Protière, M.; Li, L. Core/Shell Semiconductor Nanocrystals. *Small* **2009**, *5*, 154–168.

(12) Zhou, J.; Zhu, M.; Meng, R.; Qin, H.; Peng, X. Ideal CdSe/CdS Core/Shell Nanocrystals Enabled by Entropic Ligands and Their Core Size-, Shell Thickness-, and Ligand-Dependent Photoluminescence Properties. *J. Am. Chem. Soc.* **2017**, *139*, 16556–16567.

(13) Empedocles, S. A.; Norris, D. J.; Bawendi, M. G. Photoluminescence Spectroscopy of Single CdSe Nanocrystallite Quantum Dots. *Phys. Rev. Lett.* **1996**, *77*, 3873–3876.

(14) Empedocles, S. A.; Neuhäuser, R.; Shimizu, K.; Bawendi, M. G. Photoluminescence from Single Semiconductor Nanostructures. *Adv. Mater.* **1999**, *11*, 1243–1256.

(15) Cui, J.; Beyler, A. P.; Marshall, L. F.; Chen, O.; Harris, D. K.; Wanger, D. D.; Brokmann, X.; Bawendi, M. G. Direct Probe of Spectral Inhomogeneity Reveals Synthetic Tunability of Single-Nanocrystal Spectral Linewidths. *Nat. Chem.* **2013**, *5*, 602–606.

(16) Gómez, D. E.; Van Embden, J.; Mulvaney, P. Spectral Diffusion of Single Semiconductor Nanocrystals: The Influence of the Dielectric Environment. *Appl. Phys. Lett.* **2006**, *88*, No. 154106.

(17) Park, Y.-S.; Lim, J.; Klimov, V. I. Asymmetrically Strained Quantum Dots with Non-Fluctuating Single-Dot Emission Spectra and Subthermal Room-Temperature Linewidths. *Nat. Mater.* **2019**, *18*, 249–255.

(18) Liptay, T. J.; Marshall, L. F.; Rao, P. S.; Ram, R. J.; Bawendi, M. G. Anomalous Stokes Shift in CdSe Nanocrystals. *Phys. Rev. B* **2007**, *76*, No. 155314.

(19) Takagahara, T. Electron-Phonon Interactions in Semiconductor Nanocrystals. *J. Lumin.* **1996**, *70*, 129–143.

(20) Nomura, S.; Kobayashi, T. Exciton-LO-Phonon Couplings in Spherical Semiconductor Microcrystallites. *Phys. Rev. B* **1992**, *45*, 1305–1316.

(21) Patrick, C. E.; Giustino, F. Quantum Nuclear Dynamics in the Photophysics of Diamondoids. *Nat. Commun.* **2013**, *4*, No. 2006.

(22) Stoneham, A. M. *Theory of Defects in Solids*; Oxford University Press: Oxford, 1975.

- (23) Alkauskas, A.; Lyons, J. L.; Steiauf, D.; Van de Walle, C. G. First-Principles Calculations of Luminescence Spectrum Line Shapes for Defects in Semiconductors: The Example of GaN and ZnO. *Phys. Rev. Lett.* **2012**, *109*, No. 267401.
- (24) Kang, Y.; Nahm, H.-H.; Han, S. Light-Induced Peroxide Formation in ZnO: Origin of Persistent Photoconductivity. *Sci. Rep.* **2016**, *6*, No. 35148.
- (25) Fernée, M. J.; Littleton, B. N.; Cooper, S.; Rubinsztein-Dunlop, H.; Gómez, D. E.; Mulvaney, P. Acoustic Phonon Contributions to the Emission Spectrum of Single CdSe Nanocrystals. *J. Phys. Chem. C* **2008**, *112*, 1878–1884.
- (26) Muljarov, E. A.; Zimmermann, R. Dephasing in Quantum Dots: Quadratic Coupling to Acoustic Phonons. *Phys. Rev. Lett.* **2004**, *93*, No. 237401.
- (27) Alkauskas, A.; Buckley, B. B.; Awschalom, D. D.; Van de Walle, C. G. First-Principles Theory of the Luminescence Lineshape for the Triplet Transition in Diamond NV Centres. *New J. Phys.* **2014**, *16*, No. 073026.
- (28) Makram-Ebeid, S.; Lannoo, M. Quantum Model for Phonon-Assisted Tunnel Ionization of Deep Levels in a Semiconductor. *Phys. Rev. B* **1982**, *25*, 6406–6424.
- (29) Huang, K.; Rhys, A. Theory of Light Absorption and Non-Radiative Transitions in F-Centres. *Proc. R. Soc. London, Ser. A* **1950**, *204*, 406–423.
- (30) Han, P.; Bester, G. Fundamental Difference between Measured and Calculated Exciton-Phonon Coupling in Nanostructures. *Phys. Rev. B* **2019**, *99*, No. 100302(R).
- (31) Kresse, G.; Furthmüller, J. Efficient Iterative Schemes for Ab Initio Total-Energy Calculations Using a Plane-Wave Basis Set. *Phys. Rev. B* **1996**, *54*, 11169–11186.
- (32) Kresse, G.; Joubert, D. From Ultrasoft Pseudopotentials to the Projector Augmented-Wave Method. *Phys. Rev. B* **1999**, *59*, 1758–1774.
- (33) Perdew, J. P.; Burke, K.; Ernzerhof, M. Generalized Gradient Approximation Made Simple. *Phys. Rev. Lett.* **1996**, *77*, 3865–3868.
- (34) Dudarev, S.; Botton, G.; et al. Electron-Energy-Loss Spectra and the Structural Stability of Nickel Oxide: An LSDA+U Study. *Phys. Rev. B* **1998**, *57*, 1505–1509.
- (35) Tiago, M. L.; Ismail-Beigi, S.; Louie, S. G. Photoisomerization of Azobenzene from First-Principles Constrained Density-Functional Calculations. *J. Chem. Phys.* **2005**, *122*, No. 094311.
- (36) Zang, X.; Lusk, M. T. Designing Small Silicon Quantum Dots with Low Reorganization Energy. *Phys. Rev. B* **2015**, *92*, No. 035426.
- (37) Kaduk, B.; Kowalczyk, T.; Van Voorhis, T. Constrained Density Functional Theory. *Chem. Rev.* **2012**, *112*, 321–370.
- (38) Gavnholt, J.; Olsen, T.; Englund, M.; Schiøtz, J.  $\Delta$ Self-Consistent Field Method To Obtain Potential Energy Surfaces of Excited Molecules on Surfaces. *Phys. Rev. B* **2008**, *78*, No. 075441.
- (39) Yu, W. W.; Qu, L.; Guo, W.; Peng, X. Experimental Determination of the Extinction Coefficient of CdTe, CdSe, and CdS Nanocrystals. *Chem. Mater.* **2003**, *15*, 2854–2860.
- (40) Ithurria, S.; Talapin, D. V. Colloidal Atomic Layer Deposition (c-ALD) Using Self-Limiting Reactions at Nanocrystal Surface Coupled to Phase Transfer between Polar and Nonpolar Media. *J. Am. Chem. Soc.* **2012**, *134*, 18585–18590.
- (41) Hines, D. A.; Kamat, P. V. Recent Advances in Quantum Dot Surface Chemistry. *ACS Appl. Mater. Interfaces* **2014**, *6*, 3041–3057.
- (42) Won, Y.-H.; Cho, O.; Kim, T.; Chung, D.-Y.; Kim, T.; Chung, H.; Jang, H.; Lee, J.; Kim, D.; Jang, E. Highly Efficient and Stable InP/ZnSe/ZnS Quantum Dot Light-Emitting Diodes. *Nature* **2019**, *575*, 634–638.
- (43) Chang, J. H.; Park, P.; Jung, H.; Jeong, B. G.; Hahm, D.; Nagamine, G.; Ko, J.; Cho, J.; Padilha, L. A.; Lee, D. C.; Lee, C.; Char, K.; Bae, W. K. Unraveling the Origin of Operational Instability of Quantum Dot Based Light-Emitting Diodes. *ACS Nano* **2018**, *12*, 10231–10239.
- (44) Mack, T. G.; Jethi, L.; Kambhampati, P. Temperature Dependence of Emission Line Widths from Semiconductor Nano-crystals Reveals Vibronic Contributions to Line Broadening Processes. *J. Phys. Chem. C* **2017**, *121*, 28537–28545.